High-Resolution Sizing of Monolayer-Protected Gold Clusters by Differential Centrifugal Sedimentation

Željka Krpetić,[†,⊥] Adam M. Davidson,[†] Martin Volk,[‡,*] Raphaël Lévy,[§] Mathias Brust,[†] and David L. Cooper[†,*]

[†]Department of Chemistry, University of Liverpool, Liverpool L69 7ZD, United Kingdom, [‡]Surface Science Research Centre, Department of Chemistry, Abercromby Square, University of Liverpool, Liverpool L69 3BX, United Kingdom, and [§]Structural and Chemical Biology, Institute of Integrative Biology, University of Liverpool, Liverpool L69 7ZB, United Kingdom. [⊥]Present address: Centre for Bio-Nano Interactions, School of Chemistry and Chemical Biology, University College Dublin, Belfield, Dublin 4, Ireland.

ABSTRACT Differential centrifugal sedimentation (DCS) has been applied to accurately size ligand-protected gold hydrosols in the 10 to 50 nm range. A simple protocol is presented to correct for particle density variations due to the presence of the ligand shell, which is formed here by either polyethylene glycol-substituted alkane thiols (PEG-alkane thiols) of different chain length or oligopeptides. The method gives reliable data for all particle sizes investigated and lends itself to rapid routine sizing of nanoparticles. Unlike TEM, DCS is highly sensitive to small changes in the thickness of the organic ligand shell and can be applied to monitor shell thickness variations of as little as 0.1 nm on particles of a given core size.

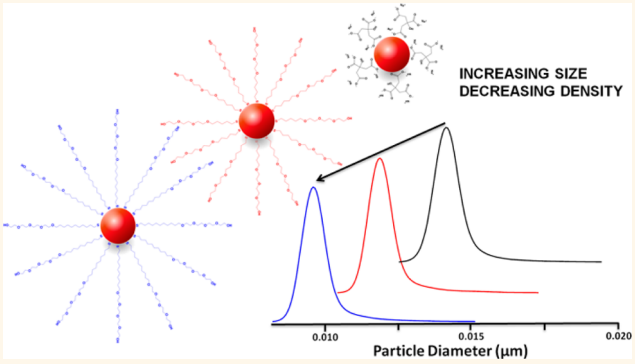

KEYWORDS: gold hydrosols · nanoparticles · differential centrifugal sedimentation (DCS) · particle sizing · monolayer-protected clusters (MPCs) · FTIR · peptide-capped nanoparticles

Many nanoparticles consist of a relatively dense and hard inorganic core surrounded by a soft shell of comparatively low density. Monolayer-protected clusters (MPCs) of gold are perhaps the most widely studied example of such materials with a vast range of current and anticipated future applications.[1−5] Key parameters that characterize a preparation of MPCs are their mean size and size distribution. Depending on the sizing methods used, this commonly refers to either the core alone or the entire particle, while an explicit distinction between the core and the ligand shell is rarely made, even though it would usually be of considerable interest. One reason for this common lack of information is that the thickness of the ligand shell cannot be measured directly by transmission electron microscopy (TEM) due to the insufficient contrast of the low-density material. Instead, it is only possible to infer estimates from measurements of the distances between the cores in densely packed assemblies of particles. Due to the unknown degree of interpenetration of the ligand shells of neighboring particles, this usually yields uncertain information as to the real thickness the ligand shell would occupy when the particles are in suspension. Given the important roles the ligands play, not only as stabilizers but also to impart chemical functionality and other properties to the particles, the availability of a routinely applicable robust method for ligand shell thickness determination is highly desirable.

Differential centrifugal sedimentation (DCS) and related techniques of analytical ultracentrifugation (AUC) are based on the ability to separate particles of the same density by mass, *i.e.*, size.[6] DCS in particular is rapidly gaining popularity for routine particle sizing,[7] as it is fast, accurate, and relatively inexpensive, resolves multimodal size distributions, and uses relatively small sample volumes. These techniques have previously been used to measure size distribution, sedimentation coefficients, and hydrodynamic radii of nanoscale polymer

* Address correspondence to m.volk@liverpool.ac.uk, dlc@liverpool.ac.uk.

Received for review July 1, 2013 and accepted September 23, 2013.

Published online September 23, 2013
10.1021/nn403350v

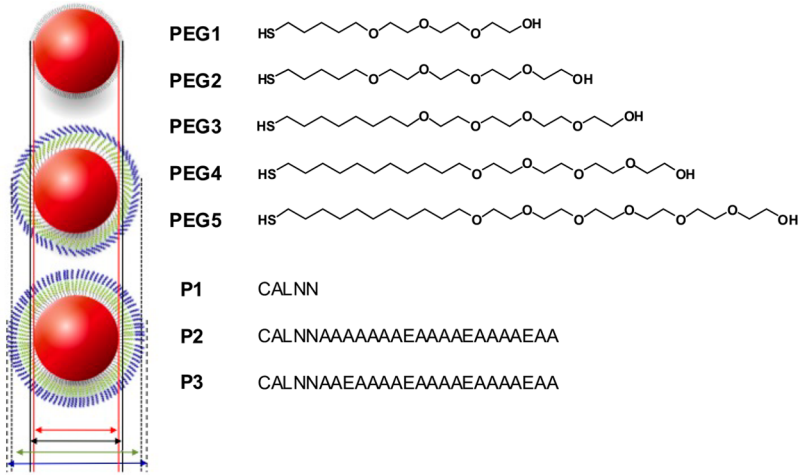

Figure 1. Ligands for nanoparticle functionalization: hydroxy PEG-thiol ligands C5EG3 (PEG1), C5EG4 (PEG2), C8EG4 (PEG3), C11EG4 (PEG4), C11EG6 (PEG5); peptides CALNN (P1), CALNNAAAAA[AAEAA]$_3$ (P2), and CALNNAAEAA[AAEAA]$_3$ (P3), with their primary sequence given in the normal one-letter code; C: cysteine, A: alanine, L: leucine, N: asparagine, E: glutamic acid. Also shown is a cartoon of the GNP1 (citrate-stabilized core), GNP1@P3, and GNP1@P2 particles, showing the relative size of core and ligand shells.

particles,[8−10] functionalized quantum dots,[11] and inorganic nanoparticles including Pt and ZnO,[12] FePt,[13] TiO_2,[14] Mn@ZnS,[15] and modified gold nanoparticles and nanocrystals.[16−18] Particles with a size difference of less than 1 Å can be resolved by these techniques.[12] In addition to particle sizing, DCS has been used to determine changes in surface structure, comparing unconjugated particles to those conjugated with biomolecules, and was recently applied in a study of binding isotherms of nanoparticles.[19] Similarly, Calabretta *et al.* showed the attachment of DNA binding protein LacI to gold nanocrystals by evaluating the changes in the sedimentation properties of hybrid nanocrystals.[18]

Here we show that DCS can be used to measure the ligand shell thickness, and we present data sets for a range of gold core diameters and ligand shells consisting of either PEGylated thiols of different lengths or oligopeptides. Importantly, the thickness measurements do not depend on independent TEM core size measurements. For a constant core size distribution, this enables us to resolve minute differences in ligand shell thickness, smaller than the statistical error associated with routine core size measurements by TEM.

RESULTS AND DISCUSSION

DCS Results. Citrate-stabilized aqueous gold nanoparticles of four different nominal core sizes, 10, 15, 20, and 45 nm (GNP1−4), were prepared and analyzed by DCS before and after modification with two different types of commonly used organic ligands, *i.e.*, peptides[20] and PEG thiols[2,21] (Figure 1). Surface modification with functional ligands was confirmed by UV−vis spectroscopy, which showed small shifts of the surface plasmon band due to the ligand attachment causing changes in the refractive index of the medium surrounding the metal core[20] (Supporting Information, Figure S1) and for some of the peptide-capped nanoparticles by Fourier transform infrared (FTIR) spectroscopy (Figure 2). Example size distributions determined by DCS are shown in Figure 3, and the raw results of all DCS measurements, *i.e.*, the apparent particle diameter reported by the DCS software, d_{DCS}, averaged over three separate measurements, are reported in Table 1. Figure S6 and Table S1 in the Supporting Information present the individual results as well as the widths of the size distributions, which were found to be in the range 10−15% of the average particle diameter for all samples. Thus, the samples used here were highly monodisperse, and we therefore mostly refer to the average particle diameter rather than the full distribution in our discussion, although our analysis of the DCS data explicitly takes account of the width of the size distribution (see Supporting Information). With the exception of GNP4 with longer PEG ligands, for which clusters consisting of two and three nanoparticles could be seen, no significant aggregation was observed in our samples.

The raw data, *i.e.*, the apparent particle diameters obtained directly from the DCS analysis (maxima of the distributions), change systematically with the length of the ligand molecules, curiously suggesting smaller particle diameters for longer ligand molecules. This is due to an oversimplification implicit in the algorithm by which the instrument attempts to calculate the particle diameter, namely, the assumption that the density of the nanoparticles is that of gold (19.3 g/cm^3). The longer the ligand molecules and the smaller the core size of the particles, the more the actual (average) density of the particles differs from this value, given that the density of the ligand shell is much lower than that of gold. This effect overcompensates for the actual increase in particle diameter with increasing ligand length and leads to the counterintuitive trend

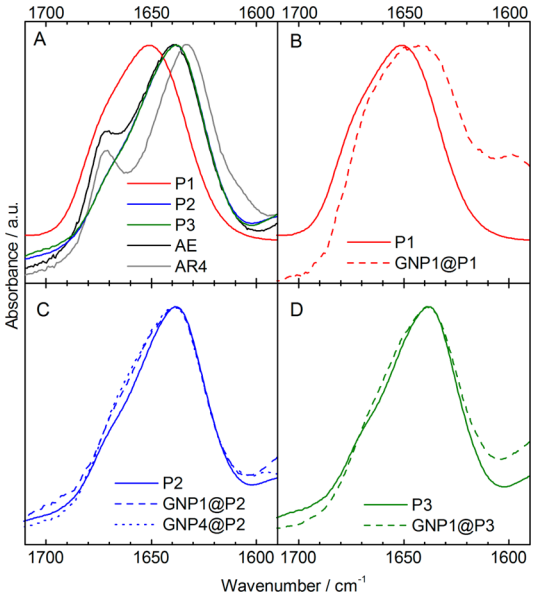

Figure 2. FTIR spectra in the amide I region. (A) Peptides in aqueous solution: P1−P3 as defined in Figure 1, compared with two helical peptides: AE (Ac-(AAEAA)$_4$GY-NH$_2$), with a helical content of 0.58,[38] and AR4 (Ac-AAAAAA(AARAA)$_4$-NH$_2$), which is expected to have an even higher helical content due to the replacement of glutamic acid by arginine with a higher helical propensity[38] (the band at 1672 cm^{-1} in the spectra of AE and AR4 originates from residual trifluoroacetic acid that had not been removed from these samples). (B−D) Peptides P1 to P3 in solution and in the capping layer of GNP1 and GNP4 (P2 only). All spectra have been normalized to the same maximum absorbance for better comparability.

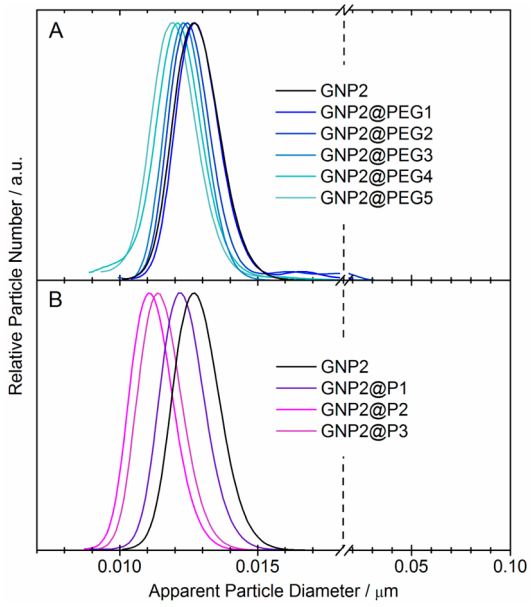

Figure 3. Normalized number size distributions of citrate-stabilized GNP2 and GNP2 with PEG-thiol (A) or peptide (B) capping layer, analyzed by DCS (similar scenarios were found for all cores; see Table 1 and Figure S6 and Table S1 in the Supporting Information), showing the shift to smaller apparent size with increasing ligand size.

observed here.[16] The reverse scenario has recently been reported and resolved by Fielding *et al.*, who studied polymer spheres surrounded by a shell of silica particles of significantly higher density than the core.[22] In either case, the results obtained directly from the instrument yield neither the true particle diameter nor that of the core, since they are based on the incorrect assumption that the particles are of uniform known density. Obviously, this shift of the apparent diameter relative to the real one also depends on the densities and would disappear in the extreme case of identical core and ligand densities, when the raw DCS data would correspond directly to the correct overall size. In the following, we report how the as-obtained (apparent) particle diameters can be used to obtain detailed information about the true core size as well as the actual shell thickness without the need for any prior assumptions about the core gold nanoparticle size.

Theory of DCS Experiments on Core−Shell Nanoparticles. Consider that each particle consists of a core of diameter d_{core} that has the density ρ_{core} and of a ligand shell of thickness s that has the density ρ_{shell}, yielding a total particle diameter $d_{core} + 2s$. The average density $\rho_{effective}$ of this particle is given by

$$\rho_{effective} = \frac{d_{core}{}^3\rho_{core} + ((d_{core}+2s)^3 - d_{core}{}^3)\rho_{shell}}{(d_{core}+2s)^3} \quad (1)$$

TABLE 1. Particle and Shell Sizes of GNP1−4 Core Particles with Different Shells,[a] Showing the Apparent Particle Diameters, d_{DCS},[b] and the Results of the Analysis, *i.e.*, the Core Diameter, d_{core}, and Shell Thickness, s;[c] Also Given Are the Values of d_{core} Averaged over All PEGylated Gold Nanoparticles

		citrate	PEG1	PEG2	PEG3	PEG4	PEG5	⟨PEG⟩	P1	P2	P3
d_{DCS}/nm[b]	GNP1	10.0	10.3	10.1	9.8	9.5	9.3		9.7	8.6	8.9
	GNP2	12.7	12.7	12.5	12.4	12.1	12.0		12.3	11.1	11.5
	GNP3	16.4	16.2	16.0	16.1	15.8	15.5		16.1	14.8	15.4
	GNP4	41.5	41.3	41.1	41.1	40.7	40.8		41.1	39.6	40.2
d_{core}/nm[c]	GNP1	10.8	11.2	11.1	10.9	10.9	10.8	11.0	10.9	10.7	10.7
	GNP2	13.5	13.6	13.5	13.5	13.6	13.6	13.6	13.5	13.3	13.4
	GNP3	17.2	17.2	17.1	17.3	17.3	17.1	17.2	17.4	17.2	17.4
	GNP4	42.4	42.3	42.2	42.4	42.4	42.6	42.4	42.5	42.5	42.5
s/nm[c]		1.00	1.15	1.30	1.45	2.00	2.15		1.60	3.55	2.80

[a] GNP1−4 were either citrate-stabilized or modified with PEG ligands [PEG1−5] or peptides [P1−3]. [b] d_{DCS} is the particle diameter reported by the DCS software (maximum of the distribution), calculated assuming a homogeneous particle density of 19.3 g/cm^3, averaged over three separate DCS runs; results for individual runs (apparent particle diameter and width of the distribution) are reported in Table S1 in the Supporting Information. [c] d_{core} is the core diameter and s is the shell thickness, obtained from our analysis, as described in the text.

Based on Stokes' law, the measured sedimentation time, t, is given by[23]

$$t = \frac{C}{(\rho_{effective} - \rho_{fluid})(d_{core}+2s)^2} \quad (2)$$

Here, ρ_{fluid} is the (average) density of the sucrose solution in which the experiment is carried out and C is a constant that depends on solution viscosity,

centrifuge spin speed, and cell geometry; in practice, C is determined using a calibration sample of known particle diameter.

On the other hand, the DCS instrument reports the diameter d_{DCS} for a fictitious particle of homogeneous density that has the same sedimentation time t. The homogeneous density of this fictitious particle needs to be supplied by the operator; here, the value of the core material (ρ_{core} = 19.3 g/cm^3) was used as the best *a priori* approximation. Thus,

$$(\rho_{effective} - \rho_{fluid})(d_{core}+2s)^2 = (\rho_{core} - \rho_{fluid})d_{DCS}^2 \quad (3)$$

It has to be noted that $\rho_{effective}$ itself depends on both d_{core} and s, eq 1, so that it is not possible to derive the values of these parameters or that of the total particle diameter (d_{core} + 2s) from the experimental result d_{DCS} without independent knowledge of at least one of them. Only if one of the values is determined independently—or its value arbitrarily assumed—can eq 3 be solved, either iteratively or using the known roots for a cubic equation.

In previous applications of DCS or AUC to the determination of nanoparticle sizes or size distributions, this problem was overcome by a variety of methods, such as measuring the core size of semiconductor quantum dots by UV−vis spectroscopy,[11] the determination of $\rho_{effective}$ by pycnometry,[15] the use of solvents with different ρ_{fluid},[13] or the determination of shell thickness and packing density using SAXS.[22] None of these methods is easily and reliably applicable to gold nanoparticles with ∼10 nm diameter: the UV−vis spectrum is not highly sensitive to size,[24] the small amount of sample precludes the use of pycnometry, and the density of gold is much higher than that of any solvent, which makes the DCS results insensitive to solvent density. TEM has also been used to determine the core size to permit AUC analysis[16] and we will comment below on the limitations associated with TEM for this purpose. Only a more advanced application of ultracentrifugation, 2D-AUC, allows the determination of the sedimentation *and* diffusion coefficient of core−shell nanoparticles, from which all parameters can be determined.[17]

In principle, it should be possible to overcome this underdetermination problem from our set of data by assuming that the ligand shell thickness is independent of the core size, which leaves only 13 independent parameters—the core sizes $d_{core,i}$ (i = 1−4) and shell thicknesses s_j (j = 1−9)—whereas 36 experimental results are available. To investigate this idea, the data were fitted in an iterative process, which is described in Materials and Methods and in more detail in the Supporting Information. We found that although the resulting ligand shell thicknesses s_j are strongly correlated and show the expected trends, *i.e.*, increasing values for longer ligands, fits of similarly good quality and consistency were possible for a wide range of values, with corresponding variations of the core sizes $d_{core,i}$ (Supporting Information, Table S2). Thus, we had to conclude that this approach is not sufficiently sensitive for the analysis of our DCS data. In the following, we will show how we were able to overcome this limitation by independently determining the thickness of the P1 (CALNN peptide) ligand shell. This allowed us to determine the core sizes d_{core} of the gold nanoparticles used in our DCS experiments, and with these values we then could determine the thickness of the other ligand shells. However, it should be noted that the shell thickness increments, *i.e.*, the differences between the thickness of different shells, are essentially the same for all of the consistent fit results (Table S2). Thus, *changes* in the shell thickness for different ligands can be measured accurately (±0.1 nm) even without this independent determination of a particular ligand shell thickness.

Thickness of CALNN Ligand Shell. The packing density of a capping layer of peptide P1 (CALNN) on gold nanoparticles, prepared following the procedure used here, has been determined to be 2.4 peptides/nm^2.[25] The minimum thickness of a compact layer of P1 can be estimated from this packing density to be 1.5 nm, using *either* the widely accepted density of polypeptides[26] of 1.4 g/cm^3 *or* the estimated volume of the CALNN peptide.[25] However, a larger thickness, *i.e.*, a less compact layer that may also contain significant amounts of solvent or cosolute molecules, cannot be ruled out *a priori*. On the other hand, the backbone of a pentapeptide can have a length of at most 1.7 nm (3.34 Å/residue),[27] which requires it to adopt a fully extended (straight) conformation. Thus, there is only a narrow range of acceptable values for the thickness of a P1 capping layer of such high packing density, and it can be concluded that peptide P1 in such a capping layer must have an almost straight backbone, although when free in solution it is in random coil conformation. Only this straight conformation, and concomitant loss of peptide backbone flexibility, allows P1 to achieve maximum packing density on the particle, limited only by steric constraints.

We previously used FTIR spectroscopy in the amide I band, which is highly sensitive to secondary structure,[28] to investigate the structure of peptide ligands on gold nanoparticles and reported the P1 ligand to be mostly in random coil conformation.[29] However, we also note that the packing density of P1 on gold nanoparticles shows significant variability depending on the exact ligand exchange procedure followed.[20,25] The FTIR spectra in Figure 2 show that P1 indeed adopts a straight conformation in the nanoparticles investigated here, which is compatible with having achieved maximized packing density. The amide I band of P1 shifts from 1651 cm^{-1} (with a shoulder at ∼1675 cm^{-1}) when free in solution toward 1643 cm^{-1}

when attached to a gold nanoparticle. The former is typical for the random coil conformation, whereas the latter indicates that the peptide has adopted the polyproline II (PPII) conformation in the particle capping layer,[30,31] *i.e.*, an almost straight conformation with an extension of 0.31 nm/residue[32] or 1.6 nm overall for P1. We note that, for P1, FTIR data were collected only on GNP1, *i.e.*, the nanoparticles with highest surface curvature for which the largest degree of disorder could be expected, since more volume is available for the peptide end than near the nanoparticles surface. The fact that even for these small nanoparticles a straight conformation is found supports the assumption of a ligand shell thickness that is independent of nanoparticles size. The same conclusion can be drawn for the helical peptides, whose structure is shown to be independent of particle size by the FTIR results; see below.

Analysis of DCS Results. This independent determination of the P1 ligand shell thickness allows us to determine the core sizes d_{core} of the gold nanoparticles used in our DCS experiments based on the results of the iterative fitting procedure mentioned above. Table S2B (Supporting Information) shows that the measured apparent particle diameters, d_{DCS}, for P1-modified nanoparticles, as reported by the DCS software, are compatible with a shell ligand thickness of 1.6 nm for actual core sizes, d_{core}, of 10.9, 13.5, 17.4, and 42.5 nm for GNP1−4, respectively.

Moreover, these results also allow us to establish the values of the thickness of the other ligand shells, s_j, from the results of the iterative fitting procedure, since consistent results for the core sizes are obtained only for well-defined values of s_j, once the value for one ligand shell (and hence the core sizes) is known (Table S2). The final results, *i.e.*, the values of s_j and $d_{core,i}$ giving the most consistent results for each ligand shell, based on a P1 shell thickness of 1.6 nm, are summarized in Table 1. It can be seen that the core sizes vary only by ±0.2 nm, which is the accuracy of our method for core size determination, whereas the ligand shells can be determined with an accuracy of better than ±0.1 nm.

The core sizes thus determined can be compared to values found using TEM of 12.1, 15.0, and 19.1 nm for GNP1−3, respectively (Supporting Information, Figure S2), which are slightly larger than those obtained by DCS. It has been noted previously that TEM as a method for determining the exact value of the ensemble average of nanoparticle sizes suffers from a range of problems, such as the small sampling size (limited to hundreds of nanoparticles), potential self-selection of nanoparticles of similar sizes into larger areas on the TEM grids, and the difficulty of clearly identifying the particle edge.[16,17,22] The latter issue is demonstrated in more detail in Figure S3 in the Supporting Information. Furthermore, unlike DCS, TEM does not give access to measuring the shell thickness of organic capping ligands due to their low density and hence insufficient contrast in TEM and requires drying of the samples, thus modifying the sample condition, which may potentially change the ligand conformation from that in solution. Finally, TEM requires significant experimental effort and time. The widths of the nanoparticle size distributions obtained by DCS and TEM, on the other hand, are in good agreement, with full widths of only 10−15% for GNP1−3, confirming the monodispersity of the nanoparticle samples used here.

A widely used alternative method for determining the hydrodynamic diameter of nanoparticles is dynamic light scattering (DLS).[33] In the Supporting Information, we present results comparing size distributions of selected gold nanoparticles obtained by DCS with those obtained by DLS. Figure S4 shows that for gold nanoparticles in the 10 nm size range DLS experiments have less resolution and are significantly less reproducible than DCS experiments. In particular, DLS reports widths of the size distributions that are significantly larger than those obtained by DCS and verified by TEM (Supporting Information, Figure S4H).[33] We suggest that this is due to inherent limitations in the analysis of the measured DLS autocorrelation, which is dominated by larger particles or even small amounts of aggregates that are detected simultaneously with the smaller nanoparticles. In DCS experiments, on the other hand, particles of different sizes are physically separated before detection, which makes it much easier to overcome the problem of size-dependent scattering and absorption. It should be noted, though, that within its limited reproducibility and resolution, DLS yields values for the total particle diameter ($d_{core} + 2s$) that are in good agreement with those obtained by DCS (Supporting Information, Figure S4).

Some of the samples were also characterized by gel electrophoresis (Supporting Information, Figure S5). However, this technique is sensitive to the net charge of the nanoparticles, and thus it is not applicable to PEG-capped nanoparticles, which carry no net charge, and it does not provide quantitative information for the peptide-capped nanoparticles, whose charge state is unknown. The results do, however, confirm the relative size of the peptide-capped nanoparticles.

Several alternative methods have been used in the past for the determination of nanoparticles sizes. Similarly to DLS, fluorescence correlation spectroscopy (FCS) determines the hydrodynamic radius of nanoscale objects from the time scale of diffusion through a small laser focus. This has been used to measure the thickness of ligand layers on monodisperse inorganic cores with high resolution (0.2−0.3 nm), similar to that achieved here by DCS.[34,35] However, that method requires the addition of a fluorescence label if neither the core nor the ligands are fluorescent, as is the case for our samples. Moreover, like DLS, nanoparticles of different sizes are not physically separated and thus contribute in a complicated manner to the measured autocorrelation function, so that determining the size distributions of nonmonodisperse samples represents a significant challenge and the method can be very

sensitive to the presence of large aggregates.[34] More recently, single-particle inductively coupled plasma-mass spectrometry (spICPMS) has been developed for measuring the (core) size distribution of metal nanoparticles. Although this method has been shown to give results in close agreement with DCS (and less so with DLS results)[36] and is very well suited for the investigation of nanoparticles in complex environments at very low concentration, it is not able to detect nanoparticles below 20−30 nm diameter and does not give access to the ligand shell dimensions. Both of these techniques, FCS and spICPMS, are more advanced and time-consuming than DCS. They require specialist expertise and are not widely available, whereas DCS is a rapid method that can be used for rapid routine characterization even by a nonspecialist user.

Thickness of PEG Ligand Shells. The thickness of the PEG ligand shells (PEG1−5) could be determined with high accuracy (Table 1). It grows approximately linearly with the overall chain length (Table 1 and Supporting Information, Figure S7), with the addition of three bonds increasing the ligand shell thickness by approximately 0.2 nm, independent of the chemical nature of the additional bonds (all methylene or ethyleneglycol). This ligand shell thickness is approximately 60% of the maximum value expected for chains in all-trans conformation and oriented perpendicular to the nanoparticle surface. We also have preliminary evidence from DCS data that PEG ligand shells on silver nanoparticles have the same thickness (Supporting Information, Figure S10).

Self-assembled monolayers (SAMs) of PEG5 on a flat gold surface have been investigated previously using FTIR and X-ray photoelectron spectroscopy.[37] The thickness of these SAMs was found to be 2.5 nm, which is less than expected for the ideal structure of a PEG5 SAM on gold. The FTIR spectra confirmed that, unlike SAMs of unfunctionalized alkanethiolates, SAMs of PEG5 show a significant degree of disorder, with observable amounts of gauche conformations present in the alkane chain and the PEG moiety not exclusively adopting its preferential helical conformation.

Here, we find an even smaller value of 2.15 nm for the thickness of the PEG5 ligand shell on gold nanoparticles. It is not surprising that a nanoparticle ligand shell is even more disordered than a SAM on a flat gold surface, considering that the limited size of the flat gold facets and the significant overall curvature will reduce the driving force for forming a commensurate ligand overlayer as well as the spatial restrictions on the ligand shell.

Thickness of Helical Peptide Ligand Shells. DCS results for peptides P2 and P3 indicate a significantly different shell thickness, of 3.55 and 2.8 nm, respectively, in spite of their almost identical primary sequence and their identical secondary structure in solution, which is evidenced by their identical amide I FTIR band (Figure 2A). Comparison with results reported in the literature[38] indicates a helicity of approximately 0.6 for these peptides in solution; that is, 60% of the peptide backbone is in α-helical conformation (Figure 2A). The effect of surface curvature on peptide conformation is potentially of great interest, and we have studied this *via* FTIR.[29] Here, we found that attaching peptides P2 and P3 to nanoparticles does not greatly affect their amide I band (Figures 2C and D), so it can be concluded that, unlike P1, their average secondary structures do not significantly change on binding, remaining ∼60% helical. The identical amide I band observed for helical peptide P2 on nanoparticles with a diameter of 11 nm (GNP1) and 42 nm (GNP4), respectively (Figure 2C), moreover shows that the conformation of this peptide is independent of surface curvature.

The FTIR spectra of nanoparticles with a peptide capping layer also allow an estimate of the packing density from a comparison of the total amide I band absorption with literature values (for details see Supporting Information and Table S3). It has to be noted that this determination of the packing density from the amide absorption may to some extent be distorted by the so-called surface selection rules (SSR).[29,39] However, as discussed in detail in the Supporting Information, SSR effects are not expected to lead to a major distortion of the results; for P1 we predict a slight underestimation of the packing density due to SSR effects, whereas for P2 and P3 the values may be overestimated (by a factor of less than 1.6). The validity of this approach is confirmed by the results for the packing density of 1.7 peptides/nm^2 for P1 on nanoparticles of 11 nm diameter (GNP1), which compares reasonably well with the value of 2.4 peptides/nm^2 measured using amino acid analysis,[25] especially when taking into account the expected SSR effects.

For the helical peptides P2 and P3, on the other hand, significantly lower packing densities of 0.58 and 0.44 peptides/nm^2, respectively, were found on GNP1. This lower packing density for helical peptides, which keep their helical structure upon binding to the nanoparticle, is not surprising, since the more compact α-helical backbone structure necessarily requires a larger peptide footprint on the anchoring surface than an extended PPII backbone. However, the packing densities determined here are significantly lower than is theoretically possible for an α-helical structure, indicating that the P2 and P3 capping layers are significantly less compact than the P1 layer. An estimate of the thickness of a *compact* layer of P2 or P3, similar to the one described above for P1, based on the measured packing density and a density of 1.4 g/cm^3 (*vide supra*) yields values of 1.5 and 1.1 nm, respectively. These values are significantly smaller than the capping layer thickness determined by DCS, indicating that a significant amount of solvent molecules and counterions are incorporated into the capping layer. Thus, whereas the short peptide P1 can be packed quite closely around a nanoparticle, the same is not possible for helical peptides, most likely

due to steric and Coulombic interactions of the large and negatively charged glutamic acid side chains. This is further confirmed by a comparison with the reported packing densities of approximately 1.5 peptides/nm^2 for α-helical peptides with uncharged methyl side chains on gold and ormosil nanoparticles.[40]

Moreover, the relative packing densities of the P2 and P3 capping layer are in quantitative agreement with the DCS results for the shell thickness, indicating that the smaller effective shell thickness of the P3 layer is mostly due to less peptide binding and not due to secondary effects such as different solvation or counterion binding. Apparently, the additional (bulky and charged) glutamic acid side chain of P3, which is close to the peptide N-terminus and hence the nanoparticle surface, further increases the average peptide−peptide distance on the nanoparticle surface due to the additional steric and Coulombic interactions, compared to P2. The different shell thickness of the P2 and P3 capping layers indicates a different structural arrangement of the peptide helices. It has to be noted that the average helix length in these peptides is 2.3 nm, which fits well within the measured shell thickness even for P3, especially considering that there is no *a priori* reason why the helix axis should be perpendicular to the nanoparticle surface. Our DCS results suggest that the higher packing density of P2 leads to a structural arrangement in which the helices are forced to be, on average, more upright than for the more loosely packed P3, thus leading to a larger effective shell thickness. These observations are highly relevant for the future development of directed design criteria for peptide-capped nanoparticles.

CONCLUSIONS

We have demonstrated how DCS can be used to determine the particle sizes of ligand-stabilized gold hydrosols rapidly and with great precision. PEG- and peptide-stabilized gold nanoparticles that differ in total diameter by as little as 0.1 nm were readily distinguished by this technique. We chose to use a range of gold nanoparticles with different sizes in our study and obtained consistent results for all of them. However, it should be stressed that the availability of different nanoparticle sizes is not required for applying this method; in the simplest application, one nanoparticle core with two different ligands could be investigated.

DCS can be used to detect particles with a wide range of sizes (2 nm to 50 μm), made of any material whose density is different from that of the solvent, although the lower limit of observable particle sizes increases when the particle and solvent density are similar.[11,13−15] Even nonspherical particles such as nanorods can be investigated with this method, although this requires an independent determination of their shape or aspect ratio. For these reasons DCS represents a valid alternative to TEM, in particular for the rapid routine analysis of monodisperse water-based colloids and, by extension, those with multimodal size distributions. An example of the analysis of a multimodal size distribution (of silver nanoparticles functionalized with PEG4) is given in the Supporting Information (Figure S10). However, even for truly polydisperse samples, it will be possible to analyze rapidly the effect of ligand exchange on the size distribution. In particular, even in the absence of a suitable "calibration" ligand (such as peptide P1 used here), DCS is an excellent method to monitor minor *changes* in the thickness of homogeneous ligand shells, which cannot normally be visualized by electron microscopy.[19] Similarly to AUC,[18] DCS is also a good method for investigating the binding of individual macromolecules to nanoparticles (Supporting Information, Figure S9).[19]

MATERIALS AND METHODS

Gold Nanoparticles. Citrate-stabilized gold hydrosols of a nominal diameter of 20 nm were obtained from BBI International. Particles of 10/15 nm nominal diameter were prepared following a modified Turkevich−Frens method.[41,42] In brief, a boiling solution of 79/30 mg (200/76 μmol) of $HAuCl_4$ trihydrate in 200/300 mL of Milli-Q water was mixed quickly with 20/9 mL of a hot (60−70 °C) 40/34 mM aqueous solution of trisodium citrate, followed by reflux for 60/30 min. The mixture was then allowed to cool to room temperature and was stirred overnight. The resulting dispersion of nanoparticles was filtered before use through a 0.45 μm Millipore filter. Particles of 45 nm nominal diameter were prepared using the 15 nm particles as seeds following the method of Liu *et al.*[43] In brief, 14 mg of $HAuCl_4$ trihydrate was dissolved in 125 mL of Milli-Q water and heated to boiling. Then 5 mL of 15 nm Au-citrate nanoparticle seeds was added, along with 0.56 mL of 38.8 mM trisodium citrate, and the mixture was boiled for 30 min. To ensure the colloidal stability, 5 mL of 38.8 mM trisodium citrate was added, and the mixture further boiled for 60 min before it was allowed to cool to room temperature and stirred overnight. The resulting dispersion of nanoparticles was filtered before use through a 0.45 μm Millipore filter. Particles were characterized by UV−vis spectroscopy, TEM, and DCS.

Functionalization of Gold Nanoparticles. The particles were surface modified with either oligopeptides (P1 = CALNN, P2 = CALNNAAAAA[AAEAA]$_3$, P3 = CALNNAAEAA[AAEAA]$_3$, Peptide Protein Research Ltd.) or mercaptopolyethylene glycol derivatives of different lengths (PEG1−5: HS-$(CH_2)_x$EG$_y$-OH; x = 5, 8, 11; y = 3, 4, 6, as specified in Figure 1, Prochimia), used as ligands of choice for their wide use in a number of different applications. Peptides and PEG thiols were used as received and were attached to gold nanoparticles following established procedures.[2,20,25]

In brief, peptides P1, P2, and P3 were dissolved in Milli-Q water to give 1 mg/mL stock solutions. To 1 mL of the colloidal dispersion of GNP2−4, 111.1 μL of the peptide stock solutions was added and left overnight (colloidal dispersion of GNP1 was diluted 1:1 v/v before adding the same amount of the peptide). In total, 36 mL of each gold nanoparticle colloidal dispersion was used in these reactions. The excess of unreacted peptide was removed by repetitive cycles of centrifugation and redispersion in fresh Milli-Q water, reducing the final volume to 0.5 mL. For the FTIR analysis, peptide-stabilized gold nanoparticle samples were dialyzed against Milli-Q water at pH 2.0 overnight (Spectrapor dialysis membranes with a 1000 kDa cutoff), to remove excess trifluoroacetic acid (TFA) normally present in the peptide solutions, then twice against Milli-Q

water and finally against D_2O. After dialysis, particle samples were centrifuged and redispersed in D_2O (0.2 mL) and lyophilized.

For PEGylated particles, functional thiol-PEG ligands were dissolved in methanol to give 0.1 M stock solutions. A calculated amount of PEG ligands was added to 10 mL of as-prepared gold colloids in order to reach 20500/46100/82000/415200 functional molecules per particle depending on the particle core (GNP1/GNP2/GNP3/GNP4), and the mixture was shaken overnight. Excess ligands were removed by three cycles of centrifugation and subsequent redispersion in fresh Milli-Q water.

UV–Vis Spectroscopy. UV–vis spectra were recorded on a spectrophotometer (Thermo Scientific Genesys 20-S), registering the spectra in the 400–800 nm range using a quartz cuvette with a path length of 1 cm.

Transmission Electron Microscopy. Samples for TEM imaging were prepared by evaporating *ca*. 10 μL of the colloidal dispersion onto carbon-coated copper grids (Agar Scientific), 400 mesh. A JEOL JEM 2100FCs, with a Schottky Field Emitter electron source, operating at 200 kV, with a CEOS GmbH aberration corrector was used for TEM imaging in the bright field mode. For particle mean diameter determination, images were processed using Image-J 1.440 software.[44]

Dynamic Light Scattering. The nanoparticle hydrodynamic diameter distribution was measured on a Malvern Nanosizer (ZSeries) using a low-volume cuvette, averaging 11 runs at 25 °C.

Differential Centrifugal Sedimentation. Particle size distributions were measured using a CPS disc centrifuge DC24000 (CPS Instruments Inc.). A gradient fluid, 8–24 wt % sucrose solution in Milli-Q water, was freshly prepared and filled successively in nine steps into the disc, rotating at a speed of 24 000 rpm (except for GNP4, where the rotating speed was set to 20 000 rpm in order to reduce potential errors due to the fast sedimentation of heavy particles), starting with the solution of highest density. Calibration was performed using poly(vinyl chloride) particles (0.377 μm, Analytik Ltd.) as calibration standard before each measurement. All samples were sonicated for 15 s before injection into the disc centrifuge, and each sample was analyzed three times to verify data reproducibility (Supporting Information, Figure S4). In the measured size range of 0–100 nm, DCS measurements showed extremely monodisperse particle distributions (Figure 3).

Iterative Fitting of Raw DCS Data. Equation 3 gives the relationship between the experimental result d_{DCS}, *i.e.*, the apparent particle size reported by the software assuming a homogeneous density (here, that of gold, ρ_{core} = 19.3 g/cm^3), and the real core size d_{core} and ligand shell thickness s; it has to be noted that $\rho_{effective}$ itself depends on both d_{core} and s, eq 1. The (average) density of the sucrose solution, ρ_{fluid}, was 1.064 g/cm^3. The ligand shell density, ρ_{shell}, was varied between this value and 1.5 g/cm^3, close to the density of polypeptides[26] of 1.4 g/cm^3; see below.

For fitting the data, we assumed that the thickness of a particular ligand shell does not change with the core size. Initially, we attempted to optimize the 13 independent parameters—the core sizes $d_{core,i}$ (i = 1–4) and shell thicknesses s_j (j = 1–9)—to yield simultaneous good agreement of the values of d_{DCS}, as calculated from eqs 1 and 3, with the experimental results for all 36 samples by minimizing the sum of the squared residuals of theoretical and experimental values (χ^2). However, we found no clear minimum of χ^2 when varying these parameters and thus had to conclude that the data did not allow the determination of core sizes and shell thickness without additional information, as described above.

For investigating this further, we employed an iterative process, which is described in more detail in the Supporting Information. Briefly, the process starts by assuming a value for the citrate layer thickness, $s_{citrate}$, which allows calculation of the core sizes of GNP1–4 from the fictitious diameters, d_{DCS}, reported by the DCS instrument for citrate-stabilized particles, using eqs 1 and 3. The thickness of the other ligand shells is then varied, in each case again calculating the core sizes of GNP1–4 from the fictitious diameters, d_{DCS}, until consistent results are obtained for the core sizes of samples using different ligand shells. This process was repeated for values of $s_{citrate}$ from 0 to 1.8 nm in steps of 0.2 nm. For each choice of $s_{citrate}$, it was possible to obtain an internally consistent set of core sizes (Table S2), which is consistent with the observation that no clear minimum of χ^2 can be found in a least-squares residual fit. However, we find that the *differences* in shell thicknesses are not very sensitive to the value assumed for $s_{citrate}$. As discussed above, the value of the shell thickness of ligand P1 can be determined independently to be 1.6 nm. This allows us to select the iterative fit results obtained for $s_{citrate}$ = 1.0 nm as the optimum set of results, and these results are reported in Table 1.

Variation of the ligand shell density, ρ_{shell}, between 1.064 and 1.5 g/cm^3 did not significantly affect the fit results, as reported previously;[16] the resulting values for d_{core} and s varied by less than 0.2 and 0.05 nm, respectively (Table S2). Table 1 shows results obtained with ρ_{shell} = 1.5 g/cm^3.

FTIR Analysis. Fourier transform infrared spectra were recorded on a Bio-Rad FTS-40 FTIR spectrometer equipped with a liquid-nitrogen-cooled HgCdTe detector, averaging 500 scans with 1 cm^{-1} resolution, using an IR cell with CaF_2 windows and 50 μm spacer. Samples were suspended in D_2O to avoid the strong absorbance band of H_2O, which overlaps with the peptide amide I band. Solvent exchange was achieved by successive centrifugation, resuspension in D_2O, and repeated lyophilization from D_2O. The concentration of nanoparticles in these samples was determined from the absorbance in the plasmon resonance band near 520 nm to be 2.5–5 μM for GNP1 and 0.17 μM for GNP4, using the known extinction coefficients[24] for nanoparticles with diameters of 11 and 42 nm, respectively. For free peptide samples, dialysis and lyophilization were used to remove residual TFA and to exchange H_2O against D_2O. Typically, a concentration in the range 5–10 mg/mL was used for these samples. All spectra were corrected to yield a flat spectrum in the region 2000–1800 cm^{-1} by subtracting an appropriately scaled spectrum of D_2O. Packing densities of the peptides on the nanoparticles were determined from the amide I band area, which was measured using band fitting as described in detail in the Supporting Information.

Conflict of Interest: The authors declare no competing financial interest.

Acknowledgment. This research received funding from the European Community Seventh Framework Programme (FP7-NMP-2010-EU-MEXICO) and CONACYT under grant agreements nos. 263878 and 125141, respectively. Access to a CPS disc centrifuge was generously provided by the Knowledge Centre for Materials Chemistry (KCMC) at the University of Liverpool. We would like to acknowledge S. Romani (Centre for Materials and Structures, Department of Engineering, University of Liverpool) for use of the TEM and J. Slupsky and A. Pettitt (Department of Molecular and Clinical Cancer Medicine, University of Liverpool) for providing the Alemtuzumab antibody. We are most grateful to S. Chadwick for the synthesis and DCS investigation of antibody–nanoparticle conjugates.

Supporting Information Available: S1. Gold nanoparticle characterization (UV–vis spectroscopy, TEM, dynamic light scattering, and gel electrophoresis); S2. Raw DCS results; S3. Iterative fitting of DCS results (method details and results); S4. FTIR analysis (determination of peptide secondary structure and packing density, effect of surface selection rules); S5. DCS results for antibody binding to gold nanoparticles; S6. DCS results for silver nanoparticles. This material is available free of charge *via* the Internet at http://pubs.acs.org.

REFERENCES AND NOTES

1. Daniel, M. C.; Astruc, D. Gold Nanoparticles: Assembly, Supramolecular Chemistry, Quantum-Size-Related Properties, and Applications toward Biology, Catalysis, and Nanotechnology. *Chem. Rev.* **2004**, *104*, 293–346.
2. Kanaras, A. G.; Kamounah, F. S.; Schaumburg, K.; Kiely, C. J.; Brust, M. Thioalkylated Tetraethylene Glycol: A New Ligand for Water Soluble Monolayer Protected Gold Clusters. *Chem. Commun.* **2002**, 2294–2295.
3. Templeton, A. C.; Wuelfing, M. P.; Murray, R. W. Monolayer Protected Cluster Molecules. *Acc. Chem. Res.* **2000**, *33*, 27–36.

4. Harkness, K. M.; Turner, B. N.; Agrawal, A. C.; Zhang, Y.; McLean, J. A.; Cliffel, D. E. Biomimetic Monolayer-Protected Gold Nanoparticles for Immunorecognition. *Nanoscale* **2012**, *4*, 3843–3851.
5. Sperling, R. A.; Rivera Gil, P.; Zhang, F.; Zanella, M.; Parak, W. J. Biological Applications of Gold Nanoparticles. *Chem. Soc. Rev.* **2008**, *37*, 1896–1908.
6. Cölfen, H. Analytical Ultracentrifugation of Nanoparticles. In *Encyclopedia of Nanoscience and Nanotechnology Vol. 1*; Nalwa, H. S., Ed.; American Scientific Publishers: Stevenson Ranch, 2004; pp 67−88.
7. Krpetić, Ž.; Singh, I.; Su, W.; Guerrini, L.; Faulds, K.; Burley, G. A.; Graham, D. Directed Assembly of DNA-Functionalized Gold Nanoparticles Using Pyrrole-Imidazole Polyamides. *J. Am. Chem. Soc.* **2012**, *134*, 8356–8359.
8. Mächtle, W. High-Resolution, Submicron Particle Size Distribution Analysis Using Gravitational-Sweep Sedimentation. *Biophys. J.* **1999**, *76*, 1080–1091.
9. Müller, H. G. Determination of Very Broad Particle Size Distributions *via* Interferences Optics in the Analytical Ultracentrifuge. *Prog. Colloid Polym. Sci.* **2004**, *127*, 9–13.
10. Müller, H. G. Determination of Particle Size Distributions of Swollen (Hydrated) Particles by Analytical Ultracentrifugation. *Prog. Colloid Polym. Sci.* **2006**, *131*, 121–125.
11. Lees, E. E.; Gunzburg, M. J.; Nguyen, T.-L.; Howlett, G. J.; Rothacker, J.; Nice, E. C.; Clayton, A. H. A.; Mulvaney, P. Experimental Determination of Quantum Dot Size Distributions, Ligand Packing Densities, and Bioconjugation Using Analytical Ultracentrifugation. *Nano Lett.* **2008**, *8*, 2883–2890.
12. Cölfen, H.; Pauck, T. Determination of Particle Size Distributions with Angström Resolution. *Colloid Polym. Sci.* **1997**, *275*, 175–180.
13. Svedberg, E. B.; Ahner, J.; Shukla, N.; Ehrman, S. H.; Schilling, K. FePt Nanoparticle Hydrodynamic Size and Densities from the Polyol Process as Determined by Analytical Ultracentrifugation. *Nanotechnology* **2005**, *16*, 953–956.
14. Ramirez-Garcia, S.; Chen, L.; Morris, M. A.; Dawson, K. A. A New Methodology for Studying Nanoparticle Interactions in Biological Systems: Dispersing Titania in Biocompatible Media Using Chemical Stabilisers. *Nanoscale* **2011**, *3*, 4617–4624.
15. Dieckmann, Y.; Cölfen, H.; Hofmann, H.; Petri-Fink, A. Particle Size Distribution Measurements of Manganese-Doped ZnS Nanoparticles. *Anal. Chem.* **2009**, *81*, 3889–3895.
16. Jamison, J. A.; Krueger, K. M.; Yavuz, C. T.; Mayo, J. T.; LeCrone, D.; Redden, J. J.; Colvin, V. L. Size-Dependent Sedimentation Properties of Nanocrystals. *ACS Nano* **2008**, *2*, 311–319.
17. Carney, R. P.; Kim, J. Y.; Qian, H.; Jin, R.; Mehenni, H.; Stellacci, F.; Bakr, O. M. Determination of Nanoparticle Size Distribution Together with Density or Molecular Weight by 2D Analytical Ultracentrifugation. *Nat. Commun.* **2011**, *2*, 335–343.
18. Calabretta, M.; Jamison, J. A.; Falkner, J. C.; Liu, Y. P.; Yuhas, B. D.; Matthews, K. S.; Colvin, V. L. Analytical Ultracentrifugation for Characterizing Nanocrystals and Their Bioconjugates. *Nano Lett.* **2005**, *5*, 963–967.
19. Salvati, A.; Pitek, A. S.; Monopoli, M. P.; Prapainop, K.; Bombelli, F. B.; Hristov, D. R.; Kelly, P. M.; Aberg, C.; Mahon, E.; Dawson, K. A. Transferrin-Functionalized Nanoparticles Lose Their Targeting Capabilities When a Biomolecule Corona Adsorbs on the Surface. *Nat. Nanotechnol.* **2013**, *8*, 137–143.
20. Lévy, R.; Thanh, N. T. K.; Doty, R. C.; Hussain, I.; Nichols, R. J.; Schiffrin, D. J.; Brust, M.; Fernig, D. G. Rational and Combinatorial Design of Peptide Capping Ligands for Gold Nanoparticles. *J. Am. Chem. Soc.* **2004**, *126*, 10076–10084.
21. Bartczak, D.; Kanaras, A. G. Diacetylene-Containing Ligand as a New Capping Agent for the Preparation of Water-Soluble Colloidal Nanoparticles of Remarkable Stability. *Langmuir* **2010**, *26*, 7072–7077.
22. Fielding, L. A.; Mykhaylyk, O. O.; Armes, S. P.; Fowler, P. W.; Mittal, V.; Fitzpatrick, S. Correcting for a Density Distribution: Particle Size Analysis of Core-Shell Nanocomposite Particles Using Disk Centrifuge Photosedimentometry. *Langmuir* **2012**, *28*, 2536–2544.
23. Svedberg, T.; Nichols, J. B. Determination of Size and Distribution of Size of Particles by Centrifugal Methods. *J. Am. Chem. Soc.* **1923**, *45*, 2910–2917.
24. Haiss, W.; Thanh, N. T. K.; Aveyard, J.; Fernig, D. G. Determination of Size and Concentration of Gold Nanoparticles from UV-Vis Spectra. *Anal. Chem.* **2007**, *79*, 4215–4221.
25. Duchesne, L.; Gentili, D.; Comes-Franchini, M.; Fernig, D. G. Robust Ligand Shells for Biological Applications of Gold Nanoparticles. *Langmuir* **2008**, *24*, 13572–13580.
26. Fischer, H.; Polikarpov, I.; Craievich, A. F. Average Protein Density Is a Molecular-Weight-Dependent Function. *Protein Sci.* **2004**, *13*, 2825–2828.
27. Pauling, L.; Corey, R. B. Configurations of Polypeptide Chains with Favored Orientations around Single Bonds - 2 New Pleated Sheets. *Proc. Natl. Acad. Sci. U.S.A.* **1951**, *37*, 729–740.
28. Arrondo, J. L. R.; Muga, A.; Castresana, J.; Goñi, F. M. Quantitative Studies of the Structure of Proteins in Solution by Fourier-Transform Infrared Spectroscopy. *Prog. Biophys. Mol. Biol.* **1993**, *59*, 23–56.
29. Shaw, C. P.; Middleton, D. A.; Volk, M.; Lévy, R. Amyloid-Derived Peptide Forms Self-Assembled Monolayers on Gold Nanoparticle with a Curvature-Dependent β-Sheet Structure. *ACS Nano* **2012**, *6*, 1416–1426.
30. Petty, S. A.; Volk, M. Fast Folding Dynamics of an α-Helical Peptide with Bulky Side Chains. *Phys. Chem. Chem. Phys.* **2004**, *6*, 1022–1030.
31. Gooding, E. A.; Sharma, S.; Petty, S. A.; Fouts, E. A.; Palmer, C. J.; Nolan, B. E.; Volk, M. pH-Dependent Helix Folding Dynamics of Poly-Glutamic Acid. *Chem. Phys.* **2013**, *422*, 115–123.
32. Arnott, S.; Dover, S. D. Structure of Poly-L-Proline 2. *Acta Crystallogr., Sect. B: Struct. Crystallogr. Cryst. Chem.* **1968**, *24*, 599–601.
33. Bell, N. C.; Minelli, C.; Tompkins, J.; Stevens, M. M.; Shard, A. G. Emerging Techniques for Submicrometer Particle Sizing Applied to Stober Silica. *Langmuir* **2012**, *28*, 10860–10872.
34. Röcker, C.; Poetzl, M.; Zhang, F.; Parak, W. J.; Nienhaus, G. U. A Quantitative Fluorescence Study of Protein Monolayer Formation on Colloidal Nanoparticles. *Nat. Nanotechnol.* **2009**, *4*, 577–580.
35. Riedinger, A.; Zhang, F.; Dommershausen, F.; Roecker, C.; Brandholt, S.; Nienhaus, G. U.; Koert, U.; Parak, W. J. Ratiometric Optical Sensing of Chloride Ions with Organic Fluorophore-Gold Nanoparticle Hybrids: A Systematic Study of Design Parameters and Surface Charge Effects. *Small* **2010**, *6*, 2590–2597.
36. Pace, H. E.; Rogers, N. J.; Jarolimek, C.; Coleman, V. A.; Gray, E. P.; Higgins, C. P.; Ranville, J. F. Single Particle Inductively Coupled Plasma-Mass Spectrometry: A Performance Evaluation and Method Comparison in the Determination of Nanoparticle Size. *Environ. Sci. Technol.* **2012**, *46*, 12272–12280.
37. Harder, P.; Grunze, M.; Dahint, R.; Whitesides, G. M.; Laibinis, P. E. Molecular Conformation in Oligo(Ethylene Glycol)-Terminated Self-Assembled Monolayers on Gold and Silver Surfaces Determines Their Ability to Resist Protein Adsorption. *J. Phys. Chem. B* **1998**, *102*, 426–436.
38. Gooding, E. A.; Pozo Ramajo, A.; Wang, J.; Palmer, C.; Fouts, E.; Volk, M. The Effects of Individual Amino Acids on the Fast Folding Dynamics of α-Helical Peptides. *Chem. Commun.* **2005**, 5985–5987.
39. Donaldson, P. M.; Hamm, P. Gold Nanoparticle Capping Layers: Structure, Dynamics, and Surface Enhancement Measured Using 2D-IR Spectroscopy. *Angew. Chem., Int. Ed.* **2013**, *52*, 634–638.
40. Rio-Echevarria, I. M.; Tavano, R.; Causin, V.; Papini, E.; Mancin, F.; Moretto, A. Water-Soluble Peptide-Coated Nanoparticles: Control of the Helix Structure and Enhanced Differential Binding to Immune Cells. *J. Am. Chem. Soc.* **2011**, *133*, 8–11.
41. Turkevich, J.; Stevenson, P. C.; Hillier, J. A Study of the Nucleation and Growth Processes in the Synthesis of Colloidal Gold. *Discuss. Faraday Soc.* **1951**, *11*, 55–75.

42. Frens, G. Controlled Nucleation for Regulation of Particle-Size in Monodisperse Gold Suspensions. *Nature, Phys. Sci.* **1973**, *241*, 20–22.
43. Liu, S. H.; Han, M. Y. Synthesis, Functionalization, and Bioconjugation of Monodisperse, Silica-Coated Gold Nanoparticles: Robust Bioprobes. *Adv. Funct. Mater.* **2005**, *15*, 961–967.
44. Schneider, C. A.; Rasband, W. S.; Eliceiri, K. W. NIH Image to ImageJ: 25 Years of Image Analysis. *Nat. Methods* **2012**, *9*, 671–675.